NASA/GSFC Report on CCSDS Recommendation 2.1.8A/B Minimum Earth Station Transmitter Frequency Resolution for Spacecraft Receiver Acquisition

Wai Fong and Wing Lee

NASA/Goddard Space Flight Center
Flight Microwave and Communications Systems Branch
Mail Code 567
8800 Greenbelt Road
Greenbelt, MD 20771

February 21, 2017

Abstract

In Fall 2016, ESA presented paper SLS-RFM 16-10 documenting a possible issue with the frequency lock-in range specification in Recommendation 2.1.8A of typically 267 to 1067 Hz in considerings (b) from considerings (a) for loop bandwidths ($2B_{LO}$) in the range of 200 to 800 Hz with a recommendation of 100 Hz step size for frequency sweeping. The paper calculated the lock-in range to be ± 266 to ± 1064 rad/s or ± 42 to ± 168 Hz. Also, Recommendation 2.1.8B has the same issue for considerings (a) and (b), i.e. for $2B_{LO} = 10$ Hz, a lock-in range of 13 Hz was specified and a recommendation of 5 Hz step size for frequency sweeping. ESA also provided test results from the Rosetta and Exomars transponders. The results were somewhat inconsistent since the tests to verify lock-in and pull-in range did not include acquisition time which is vital to the definition of these performance measures. This paper will address these test results below. However, we first examine the rationale for Recommendation 2.1.8A/B and its consistency with the theory of 2nd order phase lock loop operations. Our approach is to design a digital phase locked loop (DPLL) from phase locked loop (PLL) requirements. All analysis will be performed with a DPLL.

1 Introduction

PLLs originated in 1919 [2]. Since then, the implementation of PLLs into communications hardware is commonplace with the DPLL as the preferred platform in modems. Though the origins of Recommendations 2.1.8A/B are somewhat obscure, since the input papers are no longer available, we assume that the basis for the recommendation originate from classical PLL theory [3]. Therefore, we validate these recommendations using a mixture of classical theory and the modern approach of DPLL simulations/implementations. We will focus our study on Recommendation 2.1.8A. We note that Recommendation 2.1.8B can be extrapolated from these results.

There are two distinct categories of PLL theory: linear and non-linear analyses. Within each category are two more classifications of noise and noiseless analyses. The most well understood body of analysis is the linear analysis. However, it can only approximate the acquisition time

under the noiseless case. On the other hand, noisy non-linear analysis can make good predictions for mean-time between cycle slips and the variance of the output jitter, but it cannot predict acquisition time. Since Recommendation 2.1.8A is primarily concerned with acquisition, our best tool is the noiseless linear theory though the predictions are approximate. However, we note that PLLs generally operate with large loop signal-to-noise ratios so effectively they are noiseless.

This paper has seven sections following the Introduction. Section 2 defines the PLL model and how the DPLL was designed. Section 3 discusses the formal linear theory of PLLs and DPLLs. Section 4 makes an attempt at non-linear analysis of DPLL. Section 5 defines the PLL performance measures from classical linear theory. Section 6 provides the simulation results. Section 7 correlates the results with input paper SLS-RFM 16-10. And finally, Section 8 concludes with remarks.

2 Phase Locked Loop Model

We first review the design methodology to design a 2nd order DPLL from a 2nd order PLL.

2.1 Design Methodology

The approach to DPLL design and simulation is to first start with an analog transfer function/differential equation of the PLL and then transform to discrete time/difference equation of the DPLL. This allows the user the ability to use classical control theory parameters, i.e. natural frequency, loop bandwidth and damping factor to specify performance characteristics and then simulate/design the loop with discrete digital components. Our goal is to design the loop to analyze the lock-in range given a particular loop bandwidth based on the natural frequency and damping factor. These parameters are used by convention and their definition are found in [1, 3, 2]. The model we will use is first defined with s-parameters, i.e. in Laplace transform domain. Figure 1 shows a block diagram of this model. The input is a radio frequency sine-wave with frequency of f_o and a phase offset of θ_i. The waveform is passed through a bandpass filter that only delays the signal into the detector and does not contribute to the analysis of the loop. The delay effectively adds a value of π to the phase offset. The detector is a multiplier that has a gain defined by K_d. This is followed by a control loop filter whose transfer function is $F_{LF}(s)$ which leads to a voltage controlled oscillator (VCO) gain followed immediately by the VCO transfer function of $\frac{1}{s}$. The signal is then fed back to the detector. The output of the VCO defines the phase of a cosine function whose frequency is the quiescent or expected frequency of the input sine-wave.

Through trigonometry the multiplier will produce output sine-waves that are a function of the phase sum and difference between the input sine-wave and the cosine estimate, i.e.

$$\sin(2\pi f_o t + \theta_i) \times \cos(2\pi f_o t + \theta_o) = \frac{1}{2}\sin(\theta_i - \theta_o) + \frac{1}{2}\sin(4\pi f_o t + \theta_i + \theta_o) \approx \frac{1}{2}\sin(\theta_i - \theta_o), \quad (1)$$

where f_o is the frequency of the carrier that is again assumed to be the same as the quiescent frequency of the VCO. Note, the frequency of the sum is approximately twice the input frequency and will be suppressed since the transfer function of the PLL is a low pass filter. The difference is a baseband signal and therefore will determine the operation of the PLL.

When the input sine wave is locked or acquired, the output of the multiplier is very close to zero phase, i.e. $\frac{1}{2}\sin(\theta_i - \theta_o) \approx \frac{1}{2}\theta_e$. This is called the tracking stage and PLL is operating in the linear

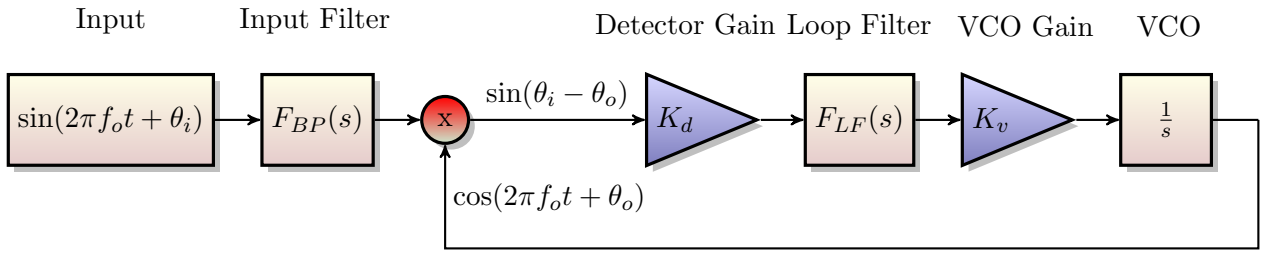

Figure 1: Simplified Analog Phase Locked Loop Model

region and this results in the approximation in (1). In general, during the acquisition mode, the PLL is operating in the non-linear region due to the output sine function of the detector. It can also be driven into the non-linear region while operating in the linear as a result of noise. For this analysis, the linear, noiseless case is only considered.

2.2 Approach

The following list of steps define how to design and simulate the loop model using Figure 1:

1. Define the performance in the analog s-domain (Laplace), i.e. specify the natural frequency ω_n, and damping factor ζ. Equivalently, the noise loop bandwidth B_L can be specified since $\omega_n = 2B_L/(\zeta + \frac{1}{4\zeta})$.

2. Set $K_d = 1/2$ (the scaling value after the multiplication of the input sine function with the cosine function from the VCO) and use the active PI loop filter $F_{LF}(s) = \frac{s\tau_2+1}{s\tau_1}$, by defining $\tau_2 = 2\zeta/\omega_n$ and $\tau_1 = 10\tau_2$. Then $K_v = \omega_n^2\tau_1/K_d$. Note steps 1 and 2 are found in [1].

3. Use the bilinear transform to convert to discrete-time z-domain, i.e.

$$s = \frac{2(z-1)}{T_s(z+1)} \tag{2}$$

   where T_s is the sampling frequency of the discrete-time PLL[1].

   The conversion of $F_{LF}(s)$ to $F_{LF}(z)$ is through the bilinear transform which is now detailed:

$$F_{LF}(z) = F_{LF}(s)\Big|_{s=\frac{2(z-1)}{T_s(z+1)}} = \frac{G_1 + G_2 z^{-1}}{1 - z^{-1}} \tag{3}$$

   where $G_1 = \frac{T_s+2\tau_2}{2\tau_1}$ and $G_2 = \frac{T_s-2\tau_2}{2\tau_1}$.

   Also, the transfer function of the VCO can be defined by combining the VCO gain with the integrator and using the bilinear transform:

[1]Note, that because the bilinear transform maps the entire s-plane from $[-\infty, \infty]$ on to the unit circle of the z-plane $[0, 2\pi]$, frequency warping will occur as the transform applies an arctan function to the mapping to avoid aliasing. In order to compensate for the distortion, prewarping is needed to ensure that effective equalization of the frequency response to largest frequency of interest ω_o, i.e. $s = \frac{\omega_o(z-1)}{\tan(\omega_o T_s/2)(z+1)}$ [6]. For the active PI DPLL, the largest frequencies of interest is at $w_o = \frac{1}{\tau_2}$ where $\tau_2 = 2\zeta/\omega_n$. Therefore, in our simulations, the largest w_o is around 50 Hz. Then $\tan(\omega_o T_s/2) = \tan(\frac{50}{8e4}) = 6.25\text{e-}4$ for $T_s = 2.5\text{e-}5$ sec, which is the same as the argument $\frac{50}{8e4} = 6.25\text{e-}4$. Therefore, it is not necessary to use the prewarping transform.

$$F_{VCO}(z) = F_{VCO}(s)\Big|_{s=\frac{2(z-1)}{T_s(z+1)}} = \frac{K_v T_s(z+1)}{2(z-1)} \tag{4}$$

4. Create difference equations for the loop using (3) and (4).
5. Simulate the PLL using Matlab.

3 Formal Analysis Using Linear Theory

This section starts the analysis using techniques developed in control theory. We begin with the classical transfer function analysis.

3.1 Frequency Transfer Functions

3.1.1 Continuous Time Transfer Functions

As a result of restricting the analysis to the linear region, transfer functions can easily be analyzed. The open loop transfer function in the s-domain is defined as [3, 1]:

$$H_o(s) = \frac{\Theta_o(s)}{\Theta_e(s)} = \frac{K_d F_{LF}(s) K_v}{s} = \frac{K_d \omega_n^2 \tau_1 (s\tau_2 + 1)}{K_d s^2 \tau_1} = \frac{\omega_n^2 (s2\zeta/\omega_n + 1)}{s^2} = \frac{s2\zeta\omega_n + \omega_n^2}{s^2} \tag{5}$$

where $\Theta_o(s)$ and $\Theta_e(s)$ are the Laplace transforms of θ_o and θ_e respectively.

The closed loop transfer function is:

$$H_c(s) = \frac{\Theta_o(s)}{\Theta_i(s)} = \frac{H_o(s)}{1 + H_o(s)} = \frac{\frac{s2\zeta\omega_n + \omega_n^2}{s^2}}{1 + \frac{s2\zeta\omega_n + \omega_n^2}{s^2}} = \frac{s2\zeta\omega_n + \omega_n^2}{s^2 + s2\zeta\omega_n + \omega_n^2} \tag{6}$$

where $\Theta_i(s)$ is the Laplace transform of θ_i.

The poles of (6) are at $s = -\omega_n(\zeta \pm \sqrt{\zeta^2 - 1})$, found by completing the square of the denominator and the zero is at $s = -\frac{\omega_n}{2\zeta}$. A plot of the poles for various values of ζ is shown in Figure 2. For $\zeta < 1$, the poles are complex pairs that approach the imaginary axis, i.e. Real$\{s\} = 0$. For $\zeta \to 0$, the response becomes more undamped and oscillatory. These values should be avoided. Note that the magnitude of the poles is always ω_n for this case, basically saying that the effect on the magnitude of the closed loop transfer function (and the error transfer function defined later) is stationary at ω_n. For $\zeta = 1$, there is a single pole on the real axis at -1. For $\zeta > 1$, the poles are real pairs. For $\zeta \geq 1$, the response is purely exponentially damped.

We can also plot the magnitude frequency response of the closed loop transfer function (6) precisely with Matlab for various values of ζ is shown in Figure 3.

The phase error transfer function is:

$$H_e(s) = \frac{\Theta_e(s)}{\Theta_i(s)} = \frac{1}{1 + H_o(s)} = \frac{1}{1 + \frac{s2\zeta\omega_n + \omega_n^2}{s^2}} = \frac{s^2}{s^2 + s2\zeta\omega_n + \omega_n^2}, \tag{7}$$

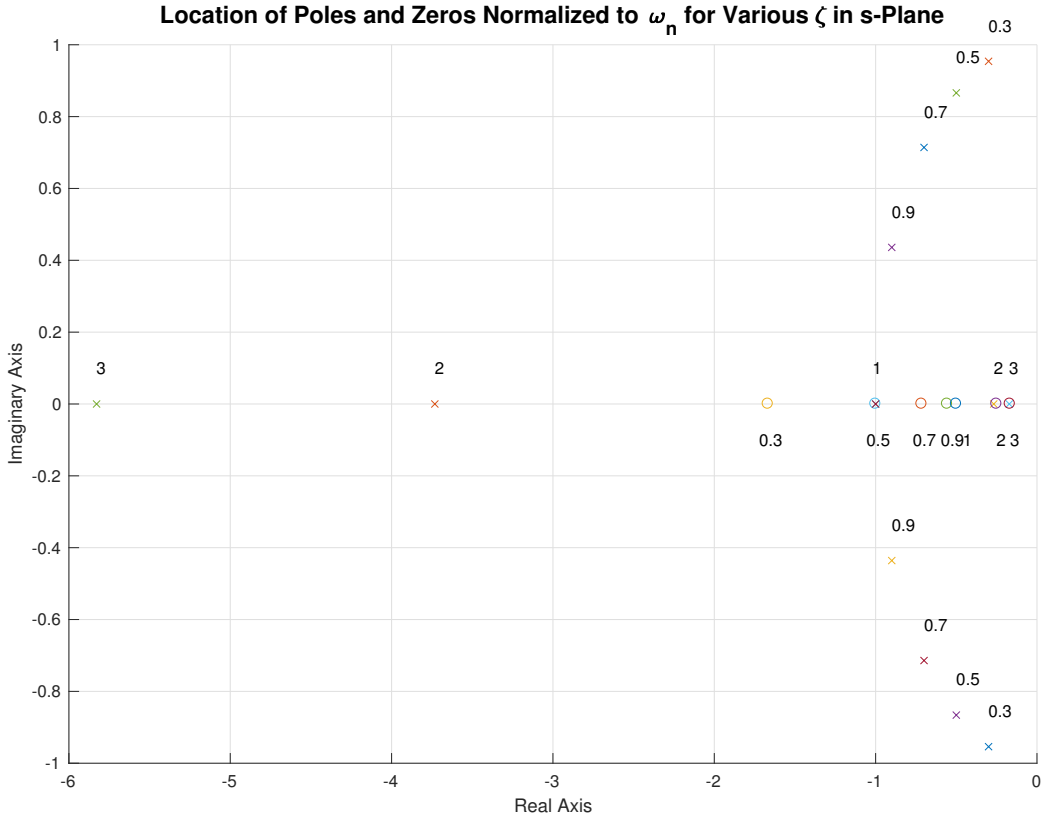

Figure 2: Location of Poles and Zeros in Complex s-Plane

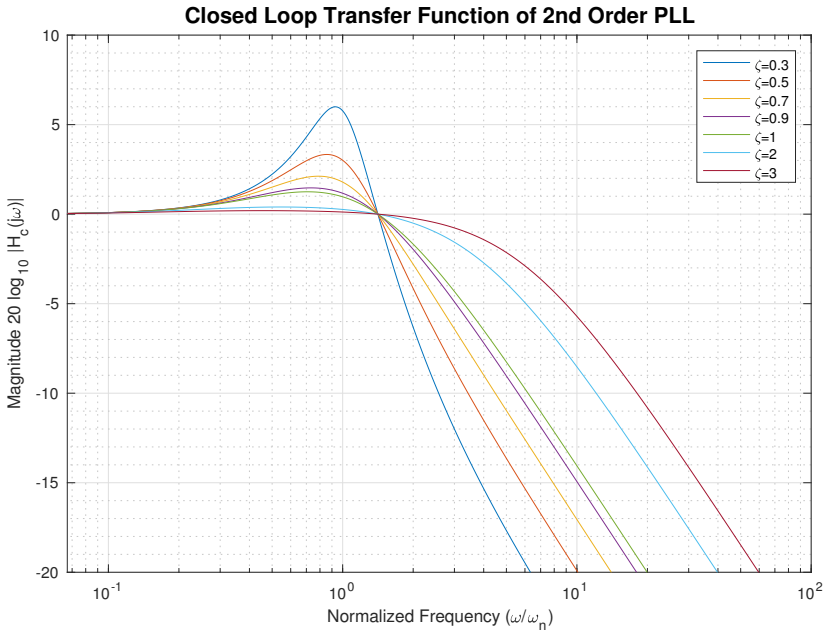

Figure 3: Closed Loop Transfer Function

note that since the denominator is the same as in the closed loop transfer function, the pole locations for both are identical. We see that there are zeros in numerator existing at location $s = 0$. The response should start at $-\infty$ for $s = 0$ and rise until the locations of the poles at $s = -\omega_n(\zeta \pm \sqrt{\zeta^2 - 1})$. In effect, the response should look like a high-pass filter with the knee at ω_n. A plot of (7) for various ζ values is shown in Figure 4.

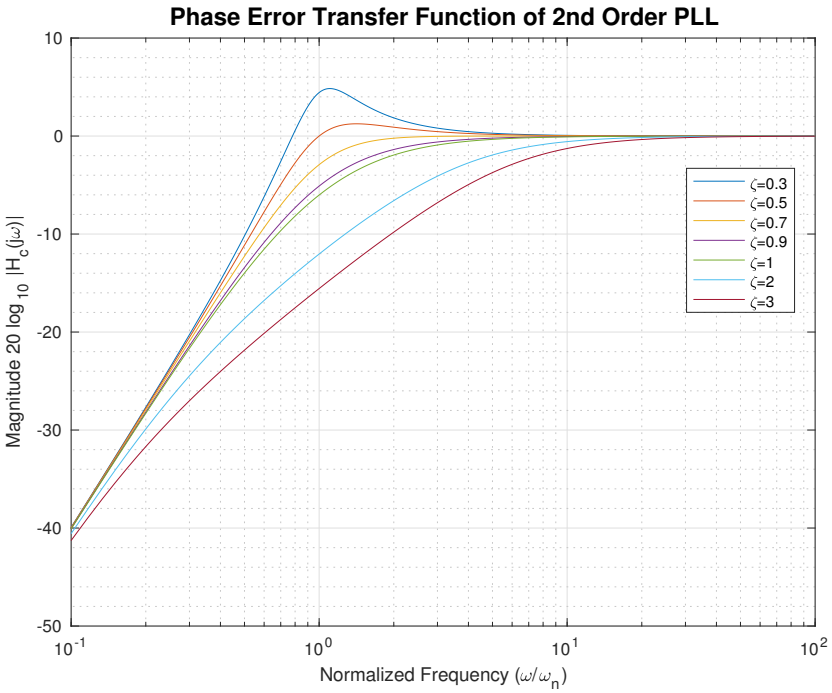

Figure 4: Phase Error Transfer Function

3.1.2 Discrete-Time Transfer Functions

The denominators of the continuous time transfer functions in (6) and (7), clearly demonstrate the second order nature of the system. We can apply the bilinear transform to the loop filter and VCO functions in both equations using (2) and get for (6):

$$H_c(z) = H_c(s)\Big|_{s=\frac{2(z-1)}{T_s(z+1)}} = \frac{\frac{2(z-1)}{T_s(z+1)}2\zeta\omega_n + \omega_n^2}{\left(\frac{2(z-1)}{T_s(z+1)}\right)^2 + \frac{2(z-1)}{T_s(z+1)}2\zeta\omega_n + \omega_n^2}. \tag{8}$$

After some algebra, we get:

$$H_c(z) = \frac{((\omega_n T_s)^2 + 4\omega_n T_s\zeta)z^2 + 2(\omega_n T_s)^2 z + (\omega_n T_s)^2 - 4\omega_n T_s\zeta}{((\omega_n T_s)^2 + 4\omega_n T_s\zeta + 4)z^2 + (2(\omega_n T_s)^2 - 8)z + (\omega_n T_s)^2 - 4\omega_n T_s\zeta + 4}. \tag{9}$$

For (7),

$$H_e(z) = H_e(s)\Big|_{s=\frac{2(z-1)}{T_s(z+1)}} = \frac{\left(\frac{2(z-1)}{T_s(z+1)}\right)^2}{\left(\frac{2(z-1)}{T_s(z+1)}\right)^2 + \frac{2(z-1)}{T_s(z+1)}2\zeta\omega_n + \omega_n^2}. \tag{10}$$

Then,

$$H_e(z) = \frac{4z^2 - 8z + 4}{((\omega_n T_s)^2 + 4\omega_n T_s\zeta + 4)z^2 + (2(\omega_n T_s)^2 - 8)z + (\omega_n T_s)^2 - 4\omega_n T_s\zeta + 4}. \tag{11}$$

As in the Laplace domain, $H_e(z) = 1 - H_c(z)$.

In Figure 5, we compare the results for $H_c(f)$ using (6) by evaluating $H_c(s)\Big|_{s=j2\pi f}$ and (8) using $H_c(z)\Big|_{z=\exp(j2\pi f T_s)}$ to show that for the most part, the equations have nearly identical frequency responses. Note that the discrete spectrum will repeat itself every $F_s = 1/T_s$ Hz due to the repetition from the transform $z = \exp(j2\pi f T_s)$. An anti-aliasing filter at the digitizer that is not shown will suppress the artifacts. However, there is some distortion in the discrete implementation before the Nyquist rate, most likely as a result of the frequency warping from the bilinear transform [6]. In this case, there is more attenuation of the stop band than predicted by the s-domain. This can be seen as beneficial to the overall performance but the transfer characteristics diverge from its -20 dB/decade decline. As demonstrated, the s-domain and z-domain responses are on top of each other prior to warping as they approach the Nyquist rate.

We can also plot the phase error transfer functions. In Figure 6, we compare (7) using $H_e(s)\Big|_{s=j2\pi f}$ and (11) using $H_e(z)\Big|_{z=\exp(j2\pi f T_s)}$. In this plot, note that the largest suppression occur at frequency below the natural frequency. Above the natural frequency results in phase errors that have little or no suppression. Also note that like the closed loop transfer function, there is a zero after the Nyquist frequency due to the spectrum repetition.

3.2 Linear Performance Predictions

We consider two inputs in the z-domain to (11), i. frequency step of $\Omega_0 T_s \frac{z}{(z-1)^2}$ and ii. frequency ramp $\Omega_1 T_s^2 \frac{z(z+1)}{2(z-1)^3}$ [2], where Ω_0 is the frequency shift at $t = 0$ in rad/sec and Ω_1 is the constant frequency ramp applied at $t = 0$ in rad/sec^2 or sec^{-2}.

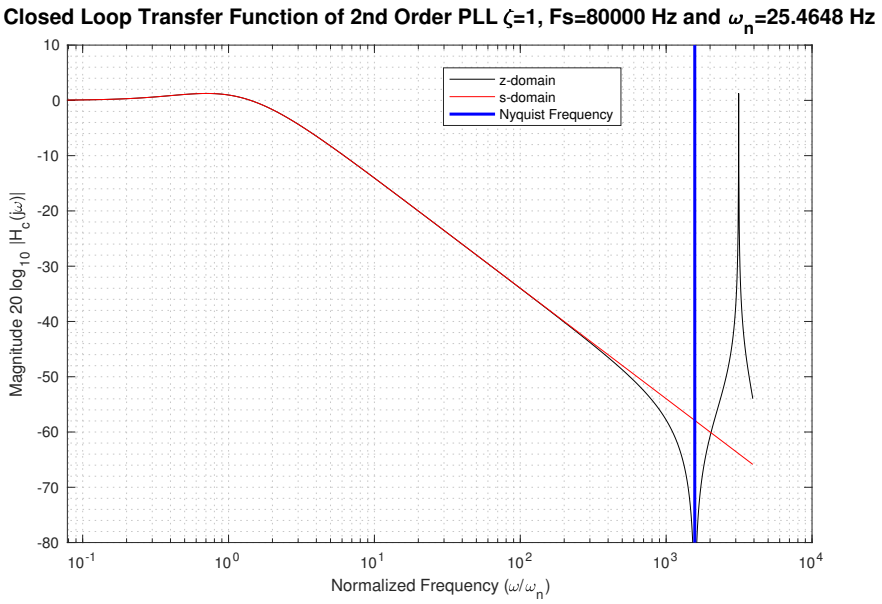

Figure 5: Closed Loop Transfer Function Magnitude Frequency Response

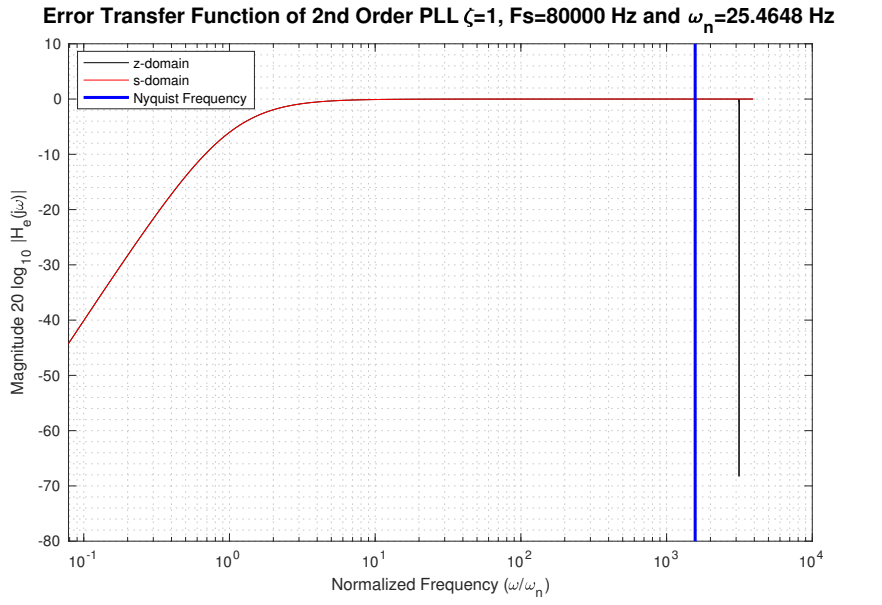

Figure 6: Phase Error Transfer Function Magnitude Frequency Response

3.2.1 Frequency Step Time Response

For the frequency step:

$$\begin{aligned}\theta_e(z) =&\Omega_0 T_s \frac{z}{(z-1)^2} H_e(z) \\ =&\Omega_0 T_s \frac{z}{(z-1)^2} \frac{4z^2-8z+4}{((\omega_n T_s)^2+4\omega_n T_s\zeta+4)z^2+(2(\omega_n T_s)^2-8)z+(\omega_n T_s)^2-4\omega_n T_s\zeta+4} \\ =&\frac{4\Omega_0 T_s z}{((\omega_n T_s)^2+4\omega_n T_s\zeta+4)z^2+(2(\omega_n T_s)^2-8)z+(\omega_n T_s)^2-4\omega_n T_s\zeta+4}.\end{aligned} \tag{12}$$

For some convenience, we write the above equation as:

$$\theta_e(z) = \frac{\frac{4\Omega_0 T_s}{(\omega_n T_s)^2+4\omega_n T_s\zeta+4} z}{z^2+2\frac{(\omega_n T_s)^2-4}{(\omega_n T_s)^2+4\omega_n T_s\zeta+4} z + \frac{(\omega_n T_s)^2-4\omega_n T_s\zeta+4}{(\omega_n T_s)^2+4\omega_n T_s\zeta+4}}. \tag{13}$$

We can use the z-transform pair:

$$\frac{az^2+bz}{z^2+2cz+d^2} \Leftrightarrow \sqrt{\frac{a^2d^2+b^2-2abc}{d^2-c^2}} d^n \cos(\omega_d n+\phi) \tag{14}$$

where $\omega_d = \arccos\left(-\frac{c}{d}\right)$, $\phi = \arctan\left(\frac{ac-b}{a\sqrt{d^2-c^2}}\right)$ and $d > 0$. For this case, $a = 0$ then (13) has a time response of:

$$\theta_e(n) = \frac{\frac{4\Omega_0 T_s}{(\omega_n T_s)^2+4\omega_n T_s\zeta+4}}{\sqrt{\frac{(\omega_n T_s)^2-4\omega_n T_s\zeta+4}{(\omega_n T_s)^2+4\omega_n T_s\zeta+4} - \left(\frac{(\omega_n T_s)^2-4}{(\omega_n T_s)^2+4\omega_n T_s\zeta+4}\right)^2}} \left(\frac{(\omega_n T_s)^2-4\omega_n T_s\zeta+4}{(\omega_n T_s)^2+4\omega_n T_s\zeta+4}\right)^{n/2} \cos(\omega_d n+\phi) \tag{15}$$

where

$$\omega_d = \arccos\left(-\frac{\frac{(\omega_n T_s)^2-4}{(\omega_n T_s)^2+4\omega_n T_s\zeta+4}}{\sqrt{\frac{(\omega_n T_s)^2-4\omega_n T_s\zeta+4}{(\omega_n T_s)^2+4\omega_n T_s\zeta+4}}}\right) \tag{16}$$

and $\phi = \arctan(-\infty) = -\pi/2$.

Then

$$\theta_e(n) = \frac{\frac{4\Omega_0 T_s}{(\omega_n T_s)^2+4\omega_n T_s\zeta+4}}{\sqrt{\frac{(\omega_n T_s)^2-4\omega_n T_s\zeta+4}{(\omega_n T_s)^2+4\omega_n T_s\zeta+4} - \left(\frac{(\omega_n T_s)^2-4}{(\omega_n T_s)^2+4\omega_n T_s\zeta+4}\right)^2}} \left(\frac{(\omega_n T_s)^2-4\omega_n T_s\zeta+4}{(\omega_n T_s)^2+4\omega_n T_s\zeta+4}\right)^{n/2} \sin(\omega_d n) \tag{17}$$

3.2.1.1 Asymptotic Analysis

Recall that the final value theorem says that for a discrete function $f[k]$ the $\lim_{k\to\infty} f[k] = \lim_{z\to 1}(z-1)F(z)$ where $F(z)$ is the z-transform of $f[k]$. Then (12) becomes,

$$\begin{aligned}\lim_{k\to\infty}\theta_e(k) &= \lim_{z\to 1}(z-1)\theta_e(z)\\ &= \lim_{z\to 1}(z-1)\frac{4\Omega_0 T_s z}{((\omega_n T_s)^2+4\omega_n T_s\zeta+4)z^2+(2(\omega_n T_s)^2-8)z+(\omega_n T_s)^2-4\omega_n T_s\zeta+4}\\ &= \lim_{z\to 1}\frac{4\Omega_0 T_s(z^2-z)}{((\omega_n T_s)^2+4\omega_n T_s\zeta+4)z^2+(2(\omega_n T_s)^2-8)z+(\omega_n T_s)^2-4\omega_n T_s\zeta+4}\\ &\to 0\end{aligned} \tag{18}$$

Thus the DPLL will have a zero phase error as time approaches infinity for any value of Ω_0. This implies that for a DPLL using an active PI loop filter, the pull-in range, i.e. the frequency range for which the DPLL will lock is infinite.

3.2.2 Frequency Ramp Time Response

For a frequency ramp, the input is: $\Omega_1 T_s^2 \frac{z(z+1)}{2(z-1)^3}$ and therefore:

$$\begin{aligned}\theta_e(z) =&\Omega_1 T_s^2\frac{z(z+1)}{2(z-1)^3}H_e(z)\\ =&\Omega_1 T_s^2\frac{z(z+1)}{2(z-1)^3}\frac{4z^2-8z+4}{((\omega_n T_s)^2+4\omega_n T_s\zeta+4)z^2+(2(\omega_n T_s)^2-8)z+(\omega_n T_s)^2-4\omega_n T_s\zeta+4}\\ =&\Omega_1 T_s^2\frac{z(z+1)}{2(z-1)}\frac{4}{((\omega_n T_s)^2+4\omega_n T_s\zeta+4)z^2+(2(\omega_n T_s)^2-8)z+(\omega_n T_s)^2-4\omega_n T_s\zeta+4}\\ =&\frac{2\Omega_1 T_s^2(z^2+z)}{(z-1)(((\omega_n T_s)^2+4\omega_n T_s\zeta+4)z^2+(2(\omega_n T_s)^2-8)z+(\omega_n T_s)^2-4\omega_n T_s\zeta+4)}\end{aligned} \tag{19}$$

At this point, we can break the equation into partial fractions and find the numerator unknowns using residues. Afterwards, we perform an inverse z-transform to each term. Since the development is quite tedious, we will not document all steps but to show the end result.

$$\theta_e(n) = \frac{\Omega_1}{\omega_n^2}\left[-\delta[n]+u[n]+A\left[\frac{(\omega_n T_s)^2-4\omega_n T_s\zeta+4}{((\omega_n T_s)^2+4\omega_n T_s\zeta+4)}\right]^{\frac{n}{2}}\cos(\omega_d n+\phi)\right] \tag{20}$$

where,

$$\omega_d = \arccos\left(-\frac{\frac{((\omega_n T_s)^2-4)}{((\omega_n T_s)^2+4\omega_n T_s\zeta+4)}}{\sqrt{\frac{(\omega_n T_s)^2-4\omega_n T_s\zeta+4}{((\omega_n T_s)^2+4\omega_n T_s\zeta+4)}}}\right), \tag{21}$$

$$\phi = \arctan\left(\frac{\frac{((\omega_n T_s)^2-4\omega_n T_s\zeta-4)}{((\omega_n T_s)^2+4\omega_n T_s\zeta+4)}\frac{((\omega_n T_s)^2-4)}{((\omega_n T_s)^2+4\omega_n T_s\zeta+4)}-\frac{((\omega_n T_s)^2-4\omega_n T_s\zeta+4)}{((\omega_n T_s)^2+4\omega_n T_s\zeta+4)}}{\frac{((\omega_n T_s)^2-4\omega_n T_s\zeta-4)}{((\omega_n T_s)^2+4\omega_n T_s\zeta+4)}\sqrt{\frac{(\omega_n T_s)^2-4\omega_n T_s\zeta+4}{((\omega_n T_s)^2+4\omega_n T_s\zeta+4)}-\left(\frac{((\omega_n T_s)^2-4)}{((\omega_n T_s)^2+4\omega_n T_s\zeta+4)}\right)^2}}\right), \tag{22}$$

and,

$$A = \sqrt{\frac{\left[\frac{((\omega_n T_s)^2-4\omega_n T_s\zeta-4)}{((\omega_n T_s)^2+4\omega_n T_s\zeta+4)}\right]^2 \frac{(\omega_n T_s)^2-4\omega_n T_s\zeta+4}{((\omega_n T_s)^2+4\omega_n T_s\zeta+4)} + \left[\frac{((\omega_n T_s)^2-4\omega_n T_s\zeta+4)}{((\omega_n T_s)^2+4\omega_n T_s\zeta+4)}\right]^2 - 2\frac{((\omega_n T_s)^2-4\omega_n T_s\zeta-4)}{((\omega_n T_s)^2+4\omega_n T_s\zeta+4)} \frac{((\omega_n T_s)^2-4)}{((\omega_n T_s)^2+4\omega_n T_s\zeta+4)} \frac{((\omega_n T_s)^2-4\omega_n T_s\zeta+4)}{((\omega_n T_s)^2+4\omega_n T_s\zeta+4)}}{\frac{(\omega_n T_s)^2-4\omega_n T_s\zeta+4}{((\omega_n T_s)^2+4\omega_n T_s\zeta+4)} - \left(\frac{((\omega_n T_s)^2-4)}{((\omega_n T_s)^2+4\omega_n T_s\zeta+4)}\right)^2}}. \tag{23}$$

Obviously, this is a very unwieldy form of the solution. The insight that can be drawn is that the response is in the form of a dampened sinusoid that will rise to final value of $\frac{\Omega_1}{\omega_n^2}$. In general, the bilinear transform produces very complex transfer and response functions but it guarantees stability in z-domain if there's stability in the s-domain. We could plot (20) but a simpler approach to finding the time response is to use (19) in Matlab and let Matlab perform the inverse. Plots of this approach for (20) and (17) respectively, are found in Figures 8 and 7 below. As demonstrated, the final values of (20) and (17), i.e. $\frac{\Omega_1}{\omega_n^2}$ and zero respectively, are approached rather quickly, i.e. within one lock time for $\zeta = 1$ and $\zeta = 0.707$.

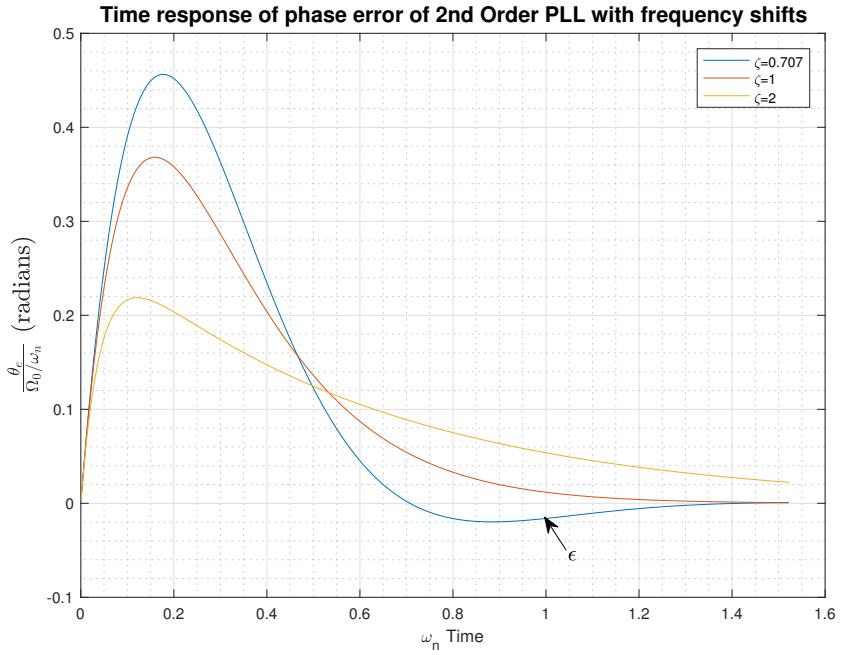

Figure 7: Time Response of 2nd Order DPLL with Frequency Shift

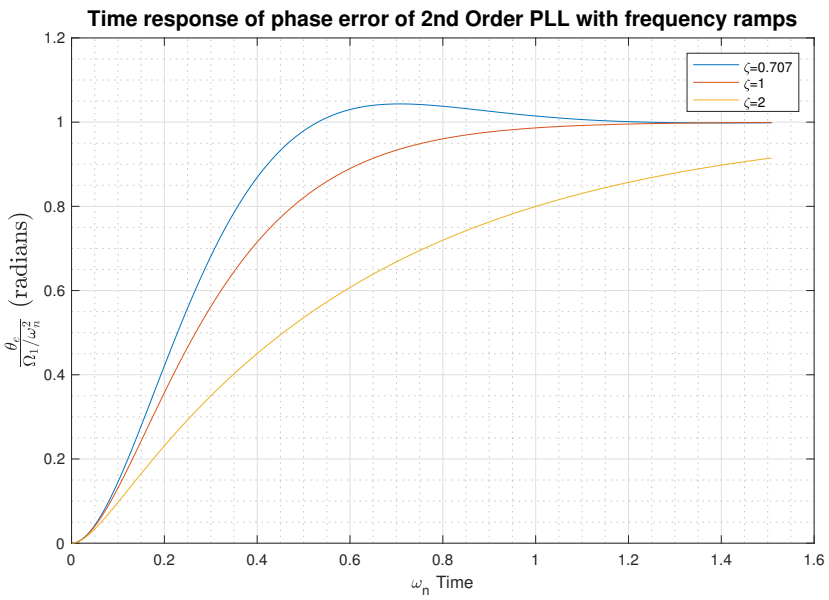

Figure 8: Time Response of 2nd Order DPLL with Frequency Ramp

3.2.2.1 Asymptotic Analysis

Using the final value theorem on the frequency ramp response, (19) becomes:

$$\begin{aligned}\lim_{k\to\infty}\theta_e(k) &= \lim_{z\to 1}(z-1)\theta_e(z)\\ &= \lim_{z\to 1}(z-1)\left[\frac{\frac{\Omega_1}{\omega_n^2}}{z-1}+\frac{\frac{\Omega_1}{\omega_n^2}((\omega_nT_s)^2-4\omega_nT_s\zeta-4)z+\frac{\Omega_1}{\omega_n^2}((\omega_nT_s)^2-4\omega_nT_s\zeta+4)}{((\omega_nT_s)^2+4\omega_nT_s\zeta+4)z^2+(2(\omega_nT_s)^2-8)z+(\omega_nT_s)^2-4\omega_nT_s\zeta+4}\right]\\ &\to\frac{\Omega_1}{\omega_n^2}\end{aligned} \tag{24}$$

According to [3], since $\theta_e(k)$ is actually limited by the sine function, its maximum value is 1 when $\theta_e(k) = \pi/2 = 1.5708$ rad. Therefore,

$$\max\Omega_1 = \omega_n^2. \tag{25}$$

Note that (18), (24) and (25) are consistent with the s-domain analysis [3].

4 Non-Linear Analysis

Up to this point, all analysis was performed based on linear methods. Non-linear analysis is considerably harder and the results are not insightful. One approach is to use a phase-plane plot of the phase error over time. Some work was done on a zero-crossing digital PLL was performed in [4]. Though in theory, an argument can be made that there is a direct relationship between this DPLL and a zero-crossing DPLL and the results can be interchanged, we will not analyze the

zero-crossing DPLL. However, we will introduce the phase-plane technique in this section and make use of it in following sections.

The difference equations that are the result of the DPLL model used can be plotted on a two-dimensional Cartesian coordinate system that begins at the initial phase and terminates when the DPLL achieves lock. We can either plot the current phase ϕ_k on the y-axis and the previous phase ϕ_{k-1} on the x-axis or plot the difference $\Delta\phi$ on the y-axis and the current phase ϕ_k. Both plots contain the same information. Figure 9 shows an example of the technique. Note that all angles are normalized to π radians. In this case, a frequency step $(\Omega_0/2\pi)$ of 130 Hz was applied to a DPLL of $\omega_n = 120$ Hz and $\zeta = 0.707$. The resulting analysis shows an acquisition time of 0.003575 seconds as each plot shows a starting point at around -1.24π radians and an end point at 0 radians.

4.1 Lock Criteria

Since a DPLL will vary its estimate when lock is reached, the criteria to determine lock must account for this variability. Therefore the criteria that was defined included a measurement accuracy of ϵ within zero radians. The most effective lock criteria was the concurrent condition that the current and the two previous phase errors all are within ϵ of zero radians. The rationale for this is that a second order loop should maintain lock for three consecutive samples. The value for ϵ was determined based on the absolute value of $\theta_e(n)$ (17) and shown in Figure 7 at arrow point based on the theoretical lock time defined below (27). The actual ϵ value used deviated slightly within a factor of around 2 from (27) since the linear behavior is an approximation. The final values were determined by reviewing the actual phase estimation plots, for example reviewing plots such as Figure 10 and determining the best values to define lock. Table 1 results are based on ϵ calculated values from (27) of -0.048 to -0.063 but the final values used were 0.02 to 0.1.

The calculated acquisition times were compared to the theoretical lock times and pull-in times. The resultant times were very accurate in regards to when the phase error settled to zero. To show the efficacy of this approach, Figure 10 shows the phase error analysis used in Figure 9. The input phase is shown in black while estimated phase is shown in red. The predicted lock time of 0.0083 (defined in Section 5.2) is shown in green and the predicted pull-in time (defined in Section 5.4) of 0.0014 seconds is shown in blue. The acquisition time of 0.003575 seconds from phase-plane analysis is shown in a thicker red line. Note, there is always a phase shift of π radians between the input phase and the estimated phase due to the delay from the input passband filter. After reviewing many simulation runs, the criteria is deemed to be sound and accurate.

5 Performance Measures Defined

References [1, 3] provide all of the following performance measures.

5.1 Lock Range

The *lock range* $\Delta\omega_L$ is "the frequency range within which a PLL locks in one single-beat note between reference frequency and output frequency."

$$\Delta\omega_L \approx \pm 2\zeta\omega_n \quad \text{radians/second.} \tag{26}$$

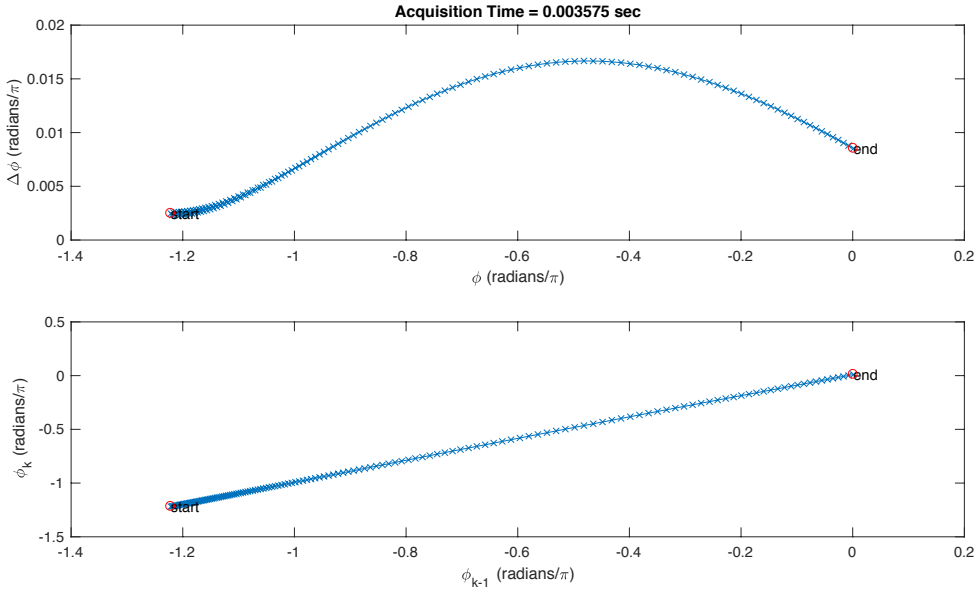

Figure 9: Phase-Plane Analysis of DPLL

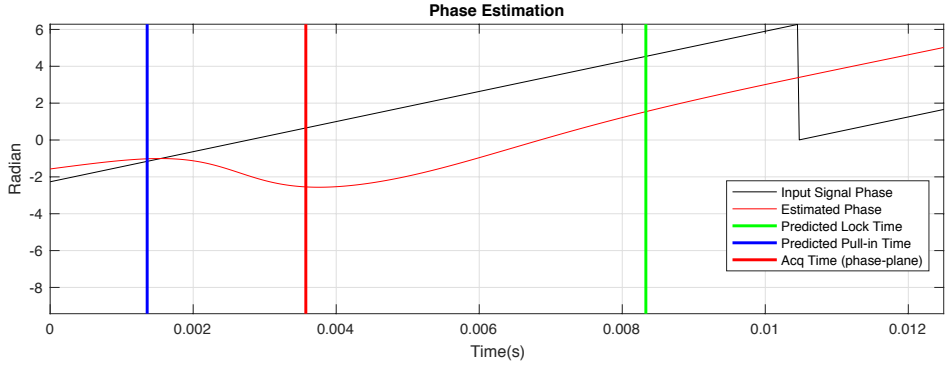

Figure 10: Phase Error Analysis

5.2 Lock Time

The *lock time* T_L is "the time the PLL needs to get locked when the acquisition process is a (fast) lock-in process." In other words, the lock time is time it takes to lock within the lock range.

$$T_L \approx \frac{2\pi}{\omega_n} \quad \text{seconds.} \tag{27}$$

5.3 Pull-in Range

The *pull-in range* $\Delta\omega_P$ is "the range which a PLL will always become locked but the process can be slow." For the active PI filter:

$$\Delta\omega_P \to \infty \quad \text{radians/second.} \tag{28}$$

5.4 Pull-in Time

The *pull-in time* T_P is "the time the PLL needs to get locked when the acquisition process is a (slow) pull-in process." For the active PI filter:

$$T_P \approx \frac{\pi^2\Omega_0^2}{16\zeta\omega_n^2} \quad \text{seconds.} \tag{29}$$

6 Simulation Results

6.1 Approach for True Lock Range Determination

Recommendation 2.1.8A is basically a recommendation of what frequency step to use at the ground when sweeping the spacecraft receiver to ensure the steps are within the lock range of the receiver. As document SLS-RFM 16-10 points out, the recommendation could be in error in specifying the step size in Hz. Our approach is to determine what the true lock range is based on a predicted lock time. We will also compare our simulated lock range to the theoretical lock range in equation (26). Then we offer conclusions and interpretations of the testing results from document SLS-RFM 16-10. The simulations are based on a DPLL engine found in [5].

To find the true lock range, we find the largest frequency step that will give an average acquisition time that is less than or equal to the predicted lock time T_L (27). We average over eight equally spaced incremental initial phase offsets from $-\pi$ to π. Recall that the acquisition time is found using the approach defined in Section 4.

6.2 Frequency Step Results

Recommendation 2.1.8A defines the noise loop bandwidth to be in the range of 100 to 400 Hz. For a $\zeta = 0.707$, our goal is to verify that the lock range is defined in (26) or $\Delta\omega_L \approx \pm 4\zeta B_L/(\zeta + \frac{1}{4\zeta})$. For $B_L = 100$ Hz, $\Delta\omega_L = 266.64$ radians/second or 42.4370 Hz. The required $\omega_n = 2B_L/(\zeta + \frac{1}{4\zeta}) =$ 188.5713 radians/sec or 30.0121 Hz. For $B_L = 400$ Hz, $\Delta\omega_L = 1.0666\text{e+}03$ radians/second or

B_L	100 Hz	200 Hz	300 Hz	400 Hz
Natural Frequency	30 Hz	60 Hz	90 Hz	120 Hz
Theoretical Lock Range	±42.4370 Hz	±84.87 Hz	±127.31 Hz	±169.7482 Hz
Lock Time	0.0333 sec	0.0167 sec	0.0111 sec	0.0083 sec
ϵ	2e-2	4e-2	6e-2	1e-1
Frequency Step	89 Hz	180 Hz	296 Hz	473 Hz
Pull-in Time	0.0407 sec	0.0208 sec	0.0167 sec	0.018 sec
Average Acquisition Times	0.0333 sec	0.0165 sec	0.0106 sec	0.0083 sec
Frequency Step	-88.7 Hz	-180 Hz	-289 Hz	-445 Hz
Pull-in Time	0.0404 sec	0.0208 sec	0.0159 sec	0.0159 sec
Average Acquisition Times	0.0334 sec	0.0166 sec	0.0105 sec	0.0085 sec

Table 1: Data Results for $\zeta = 0.707$

169.7482 Hz. The required $\omega_n = 2B_L/(\zeta + \frac{1}{4\zeta}) = 754.2852$ radians/sec or 120.0482 Hz. Lock times are $T_L \approx \frac{2\pi}{\omega_n} = 0.0333$ seconds for $B_L = 100$ Hz and $T_L = 0.0083$ seconds for $B_L = 400$ Hz.

The objective is use the lock times as a target for the average acquisition times by which we can determine the true lock range. Table 1 is a summary of the simulation results. It indicates that the theoretical lock range (26) is too narrow. For $B_L = 100$ Hz, a frequency step size of ±88 Hz will allow the DPLL to lock within the theoretical lock time as opposed to the conservative theoretical ±42.4370 Hz defined by (26). Also, for $B_L = 400$ Hz, a frequency step size of ±445 Hz will allow the DPLL to lock within the theoretical lock time as opposed to the conservative theoretical ±169.7482 Hz defined by (26). B_L values for 200 and 300 Hz are provided as well. Each column indicates that the lock range prediction (26) is too narrow. The ratios for the B_L to the true one-sided lock range are: 1.1364, 1.1111, 1.0381, and 0.8989 for 100, 200, 300, and 400 respectively. Note that the pull-in times are larger than the average acquisition times so their predictions are much less useful.

6.3 Frequency Ramp Results

For $B_L = 100$ Hz and $\zeta = 0.707$, the result of (25), i.e. $\Omega_1 = \frac{\omega_n^2}{2\pi} = 5.6594e3$, does not work. Instead a ramp of slightly lower value $\Omega_1 = \frac{0.9434\omega_n^2}{2\pi} = 5.3391e3$ sec^{-2} will work. A plot of this ramp response is shown in Figure 11. Note that the DPLL starts at phase error of π radians, i.e. the DPLL is in lock since the input passband filter has a delay of π radians. A phase error of $\pi + \pi/2$ is reached quickly as predicted by (19) and Figure 8. If we use $\zeta = 1$, again the value of $\Omega_1 = \frac{0.99\omega_n^2}{2\pi} = 4.0336e3$ sec^{-2} will work (shown in Figure 12) but $\Omega_1 = \frac{\omega_n^2}{2\pi} = 4.0744e3$ sec^{-2} does not work. This result also applies to B_L of 200, 300 and 400 Hz. After, trying various damping factors, the conclusion is that (25) is very much an approximation. The DPLL can track a ramp of $\Omega_1 = \frac{\alpha\omega_n^2}{2\pi}$ with $\alpha \lesssim 1$ for $\zeta \leq 1$ and $\alpha \gtrsim 1$ for $\zeta > 2$. We do not have an explanation for this. We speculate that for $\Omega_1 = \frac{\omega_n^2}{2\pi}$ to be achieved, the bandwidth of the transfer function has to be large enough to accommodate the frequency dynamics.

Note that it is critical that the DPLL is initially in lock. If the DPLL is not in lock, then our results show that the DPLL cannot track even for $\alpha = 0.5$.

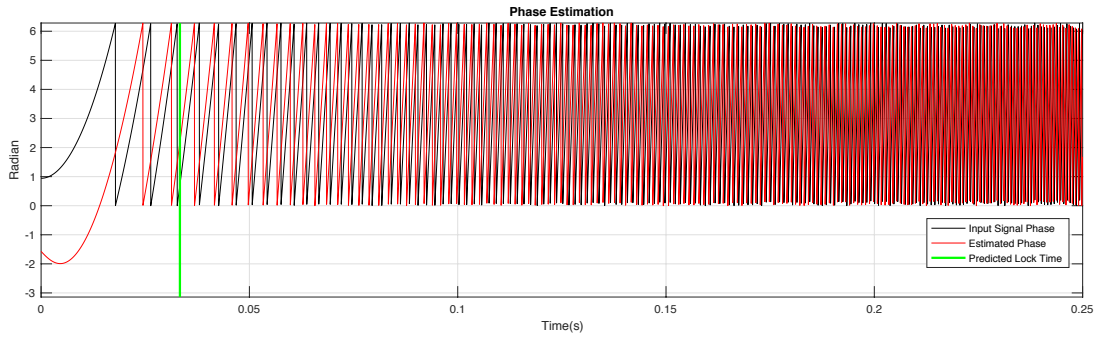

Figure 11: Frequency Ramp Response for $B_L = 100$ Hz, $\zeta = 0.707$ and $\Omega_1 = 5.3391e3$ sec^{-2}

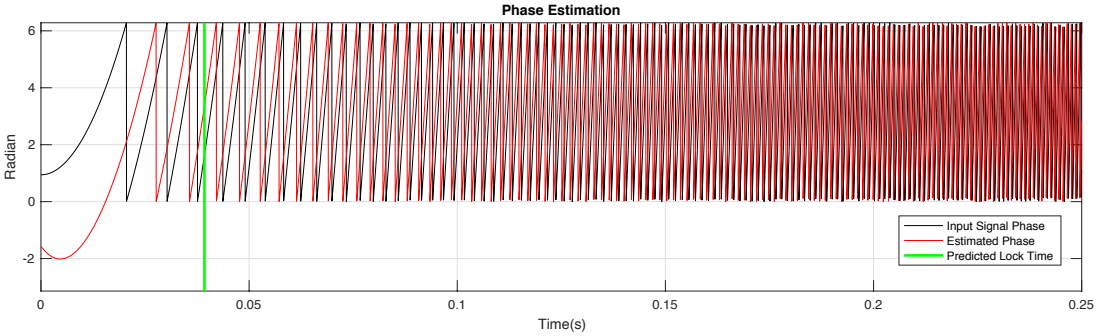

Figure 12: Frequency Ramp Response for $B_L = 100$ Hz, $\zeta = 1$ and $\Omega_1 = 4.0336e3$ sec^{-2}

7 Correlating Results with SLS-RFM 16-10

SLS-RFM 16-10 test results for Section 3.1 are difficult to interpret because there is no acquisition time recorded. The definition of lock was a declaration of lock by the receiver. Therefore we cannot correlate our results since we don't know if they achieved a pull-in range or a lock-in range. As stated before, the pull-in range for an active-PI loop filter is infinite (28). As a result, we don't understand the test measurements or the results.

From Table 1, the theoretical lock range for $B_L = 100$ and $\zeta = 0.707$ is ± 42.4370 Hz and our simulation results indicate that true lock range based on achieving the theoretical lock time is ± 88 Hz. Given that the SLS-RFM 16-10 tests do not define an acquisition time, no conclusion is drawn from comparing results. We find the same conclusion from reviewing section 3.2 of SLS-RFM 16-10.

Note, that the sweep rate tests in the annex of SLS-RFM 16-10 to measure ω_n will have some error given the simulation results in Section 6.3. Also, as noted in the previous section, frequency ramping testing must ensure that the PLL start initially in lock or else the PLL cannot maintain lock. So the results of calculating ω_n from a maximum frequency ramp is problematic as the receiver must start in lock.

8 Conclusion and Comments

We are in agreement that Recommendation 2.1.8A is probably in error for considering (b) and that recommends (1) should, in principle, be updated. Our simulations indicate that a step size of ± 88 Hz or 176 Hz should be recommended based on the smallest $2B_L = 200$ Hz. However, since the current recommendation of 100 Hz is less than 176 Hz, the recommendation still works but is not as efficient. Therefore we do not believe this is not an urgent change. Remember, that our simulation results are based on the theoretical lock time of $T_L = 2\pi/\omega_n$. If a different target lock time is agreed upon, one that maybe based on a practical time limit, then the results will change. We do, however, agree that considering (b) be updated to reflect Hz values immediately.

As an aside, Gardner [3] page 137, has stated that $\zeta < 1$ can produce clusters of cycle slips (or multiple cycle slips) that can throw the demodulator way out of lock for 2nd order PLL. We have seen these cluster slips for Costas loops and DPLLs under simulation and the clusters do reduce in likelihood for $\zeta \geq 1$. There should be some consideration to recommending $\zeta \geq 1$ when missions are concerned about cycle slips. If there is interest, we can present our findings in a future input paper.

References

[1] R. Best, *Phase-Locked Loops, 6th Ed.*, McGraw Hill, New York, NY, 2007.

[2] D. Stephens, *Phase-Locked Loops for Wireless Communications, Digital, Analog and Optical Implementations, 2nd Ed.*, Kluwer Academic Publishers, New York, NY, 2002.

[3] F. Gardner, *Phaselock Techniques, 3rd Ed.*, John Wiley and Sons, Hoboken, NJ, 2005.

[4] C.-M. Chie, *Analysis of Digital Phase-Locked Loops*, Ph.D. Dissertation, University of Southern California, January, 1977.

[5] W. Yang, Y. Cho, W. Jeon, J. Lee, J. Kim, J. Paik, M.-H. Lee, K. Lee, K. Park and K. Woo, *Matlab/Simulink for Digital Communication*, A-Jin Publishing Co., Korea, 2009.

[6] A. Oppenheim and R. Schafer, *Discrete-Time Signal Processing, 3rd Ed.*, Prentice Hall, Upper Saddle River, NJ, 2010.